eng

MDPI

Article

Analysis and Design Methodology of Radial Flux Surface-Mounted Permanent Magnet Synchronous Motors

Sergio I. Suriano-Sánchez, Mario Ponce-Silva *, Víctor H. Olivares-Peregrino, Susana E. De León-Aldaco, Abraham Claudio-Sánchez and Claudia Cortés-García

Tecnológico Nacional de México—CENIDET, Cuernavaca 62490, Morelos, Mexico; abraham.cs@cenidet.tecnm.mx (A.C.-S.); claudia.cg@cenidet.tecnm.mx (C.C.-G.)
* Correspondence: mario.ps@cenidet.tecnm.mx

Abstract: Permanent magnet motors have become very important in recent years due to the popularization of electric vehicles in the context of the efforts to transition to zero-emission transportation. This has encouraged researchers and hobbyists to learn about electric motor design. However, designing electric motors is not a simple task, as the information to achieve it is not easily available to everyone and it is usually complicated to understand. For that reason, this paper presents the equations and a basic process to design radial flux surface-mounted PM synchronous motors. This design method is the result of combining and organizing information from previous publications to create a relatively simple design guide. The result is a table of equations and a series of general guidelines that were verified by designing and simulating a 500 W eight-pole 2.6 Nm average torque dual-rotor motor and a 20 W four-pole 106 mNm single-rotor motor. The simulations validated the equations and the design method presented in this paper to be used by those interested in the field of electric motors and vehicles; therefore, in the future, others may contribute with improvements, particularizations or optimizations of this methodology, or even create their own.

Keywords: design equations; design methodology; permanent magnet motor; FEA simulation

check for updates

Citation: Suriano-Sánchez, S.I.; Ponce-Silva, M.; Olivares-Peregrino, V.H.; De León-Aldaco, S.E.; Claudio-Sánchez, A.; Cortés-García, C. Analysis and Design Methodology of Radial Flux Surface-Mounted Permanent Magnet Synchronous Motors. *Eng* **2023**, *4*, 2840–2855. https://doi.org/10.3390/eng4040160

Academic Editors: Huanyu Cheng and Thaiyal Naayagi Ramasamy

Received: 26 July 2023
Revised: 12 October 2023
Accepted: 10 November 2023
Published: 14 November 2023

1. Introduction

Energy saving is an important topic in the current times, since most electricity is still generated with nonrenewable resources, which also contaminate the environment. Moreover, industries like transportation are highly dependent on fossil fuels. One way to reduce this problem is the use of electric vehicles. For this reason, in recent years, electric vehicles have become very popular in many countries [1]; therefore, the investigation and the interest of many people in electric motors and especially permanent magnet motors have increased as a consequence. However, transportation is not the only field where electric motors are important, since they also take approximately 70% of the total energy in the industry in general, as shown in [2]. This means that the efficiency of electric motors is one of the parameters that needs to be improved by investigating new design and manufacturing methods. For this reason, it is important that more people are involved in these themes.

The main problem when trying to begin in motor design investigation is finding information about it. Electric motor design is not an easy topic, since it requires a certain level of knowledge in electromagnetic theory, magnetic circuits and electricity and, moreover, the secrecy that most paper authors have when it comes to showing the equations and the processes, followed along with a direct jump to the results section, which does not help. In most cases, the brief explanation given and the experimental or simulated results are not enough for readers to understand the process in between and to learn how to replicate those results or make their own designs and experiments. Examples of this include [3–19] where motors are designed but the detailed process is not shown.

Books like [20,21] are usually better sources of information about electric motor design, but they are often out of date, and readers, especially those who have very little experience in electric machines, can become confused by the quantity of theories, analyses, data and terminology. The lack of practical information may discourage them.

Following this context, this paper presents a methodology for the design of radial flux surface-mounted permanent magnet motors, including all the equations required. This methodology was developed by combining the magnetic model from [22,23] and the electrical and performance equations given in [21], then uniformizing and organizing all the information. The design equations and the process are presented in tables and easy-to-follow guidelines, so readers can start understanding how permanent magnet motors work, create their first simple designs and then go deeper in the matter by consulting the source references.

The structure of the paper is as follows: Section 2 first presents the main sources of information used and the advantages and disadvantages of each when it comes to show how to design permanent magnet motors. Then, the parts of the methodology and how the information from different sources was combined and uniformized are explained. After that, a list of initial parameters and design equations are presented in tables, with some design guidelines given. Next, one dual-rotor motor and one single-rotor motor are designed using the described methodology and then simulated. Section 3 shows the results obtained from the calculations and simulations. Section 4 is a discussion of the results obtained, the validity of the design methodology and future research on this topic.

2. Materials and Methods

As mentioned in the previous section, the developed design methodology was based on three main sources of information. In [22], one magnetic model for surface-mounted permanent magnet machines was developed, where various important leakage fluxes were considered, which resulted in the model being very accurate. Then, in [23], such a magnetic model was applied to design a dual-rotor motor. The problem in this last paper was that although the design of the magnetic part of the motor was sufficiently well described, the electrical part was not; therefore, the results could not be appropriately replicated, nor was the paper useful as a complete design guide. On the other hand, ref. [21] presented a complete set of equations, guidelines and the theory to complete the design of one single-rotor surface-mounted permanent magnet motor. However, the magnetic model used there was older and not as accurate as the one mentioned before, so the designs created with such a methodology would usually require several adjustments after the simulation results are obtained. Considering all these issues, the proposed design methodology combined the best from the cited references: the magnetic model from [22,23] and the electrical design equations from [21] to create a complete design methodology.

One important consideration when combining models and equations from different sources and authors is to make sure that all the analyses are compatible. This means that in the process of developing equations, no different assumptions or simplifications were determined, and, if so, we would need to recreate the analysis to ensure it was consistent with the others. Fortunately, in this case, the magnetic and electric parts of the design were almost independent, so all that was necessary was to homogenize the terms, organize the initial parameters in Table 1, and include a couple of expressions, like Equations (44) and (45) from Table 2.

Table 1. Initial parameters for design.

Parameter	Description
P	Motor output power, W
η_p	Efficiency without mechanical losses, %
S_r	Nominal speed, rpm
$E_{\max}$	Peak back-EMF, V
N_{ph}	Number of phases
N_m	Number of magnet poles
N_{sp}	Number of slots per phase
$g_{1,2}$	Air gap length, m
$R_{PM1,2}$	Radius to the upper side of the magnet, m
R_{sb1}	Stator back-iron inner radius, m
L	Motor axial length, m
$\Gamma(B_{\max}, f_e)$	Steel core loss density vs. flux density and frequency
k_{fe}, ρ_{bi}	Lamination stacking factor and steel mass density, kg/m^3
ρ	Copper resistivity
k_{cu}	Bare copper filling factor
$\alpha_{m1,2}$ o $\alpha_{mp1,2}$	Angular width of each magnet (radians) or magnet fraction w_f/τ_p
B_r	Magnet residual flux density, T
$B_{cr1,2}$	Rotor core flux density, T
B_{g1}	Air gap flux density, T
B_{cs}	Stator core flux density, T
$B_{ts1,2}$	Stator tooth flux density, T
μ_R	Magnet recoil permeability
$w_{s1,2}$	Slot opening, m
α_{sd}	Shoe depth fraction

Table 2. Design equations [21–23].

N$_o$.	Equation	Description
(1)	$\omega_m = \frac{\pi}{30} S_r$	Mechanical speed, rad/s
(2)	$\omega_e = \frac{N_m}{2} \omega_m$	Electrical speed, rad/s
(3)	$f_e = \frac{\omega_e}{2\pi}$	Fundamental electrical frequency, Hz
(4)	$T = \frac{P}{\omega_m}$	Torque from power
(5)	$N_s = N_{sp} N_{ph}$	Number of slots
(6)	$N_{spp} = \frac{N_{sp}}{N_m}$	Number of slots per pole per phase
(7)	$N_{sm} = N_{spp} N_{ph}$	Number of slots per pole
(8)	$\alpha_{cp} = \frac{\mathrm{int}(N_{spp})}{N_{spp}}$	Coil-pole fraction
(9)	$\theta_p = \frac{2\pi}{N_m}$	Angular pole pitch
(10)	$\theta_s = \frac{2\pi}{N_s}$	Angular slot pitch
(11)	$\theta_{se} = \frac{\pi}{N_{sm}}$	Slot pitch, electrical radians
(12)	$R_{is} = R_{PM1} + g_1$	Inside stator radius

Table 2. *Cont.*

N$_o$.	Equation	Description
(13)	$R_{os} = R_{PM2} - g_2$	Outside stator radius
(14)	$\tau_{p1} = R_{is}\theta_p$	Pole pitch, inner part of the motor
(15)	$\tau_{p2} = R_{os}\theta_p$	Pole pitch, outer part of the motor
(16)	$\tau_{c1,2} = \alpha_{cp}\tau_{p1,2}$	Coil pitch
(17)	$\tau_{s1} = R_{is}\theta_s$	Slot pitch at air gap, inner part of the motor
(18)	$\tau_{s2} = R_{os}\theta_s$	Slot pitch at air gap, outer part of the motor
(19)	$w_{t1,2} = \tau_{s1,2} - w_{s1,2}$	Tooth width at air gap
(20)	$k_d = \frac{\sin(N_{spp}\theta_{se}/2)}{N_{spp}\sin(\theta_{se}/2)}$	Distribution factor
(21)	$k_p = \alpha_{cp}$	Pitch factor
(22)	$k_s = 1 - \frac{\theta_{se}}{2\pi}$	Skew factor
(23)	$w_{m1,2} = R_{PM1,2}\alpha_{m1,2}$	Magnet circumferential length
(24)	$w_{f1,2} = R_{PM1,2}\theta_p - w_{m1,2}$	Circumferential length between magnets
(25)	$g_{c1,2} = g_{1,2} + \frac{H_{PM1,2}}{\mu_R}$	Effective air gap for Carter coefficient
(26)	$k_{c1,2} = \left[1 - \frac{1}{\frac{\tau_{s1,2}}{w_{s1,2}}\left(5\frac{g_{c1,2}}{w_{s1,2}}+1\right)}\right]^{-1}$	Carter coefficient
(27)	$g_{e1,2} = g_{1,2}k_{c1,2}$	Effective air gap taking into account the slotting
(28)	$\eta = \frac{H_{PM1,2}}{\pi\mu_R w_{m1,2}}\ln\left(1 + \frac{\pi g_{e1,2}}{H_{PM1,2}}\right)$	Auxiliar term for B_g y B_m
(29)	$\lambda = \frac{H_{PM1,2}}{\pi\mu_R w_{m1,2}}\ln\left(1 + \frac{\pi g_{e1,2}}{w_{f1,2}}\right)$	Auxiliar term for B_g y B_m
(30)	$B_{g1,2,ave} = \left[1 + \frac{w_{f1,2}}{w_{m1,2}} + \mu_R\frac{g_{e1,2}}{H_{PM1,2}}\frac{w_{m1,2}+w_{f1,2}}{w_{m1,2}+2g_{e1,2}}(1+2\eta+4\lambda)\right]^{-1}B_r$	Air gap flux density
(31)	$B_{m1,2} = \frac{\left(1+\frac{2g_{e1,2}}{w_{m1,2}}\right)\frac{1}{\mu_R}\frac{H_{PM1,2}}{g_{e1,2}}+2\eta+4\lambda}{\left(1+\frac{2g_{e1,2}}{w_{m1,2}}\right)\frac{1}{\mu_R}\frac{H_{PM1,2}}{g_{e1,2}}+1+2\eta+4\lambda}B_r$	Magnet working point
(32)	$d_{yr1,2} = \frac{B_{m1,2}w_{m1,2}}{2B_{cr1,2}}$	Rotor back-iron width
(33)	$R_{or1} = R_{PM1} - H_{PM1}$	Outer radius of the inner rotor
(34)	$R_{ir1} = R_{or1} - d_{yr1}$	Inner radius of the inner rotor
(35)	$R_{ir2} = R_{PM2} + H_{PM2}$	Inner radius of the outer rotor
(36)	$R_{or2} = R_{ir2} + d_{yr2}$	Outer radius of the outer rotor
(37)	$K_{Lt1,2} = 1 - \frac{\left(\tau_{s1,2}-w_{f1,2}\right)^2}{2w_{m1,2}\tau_{s1,2}}$	Air gap leakage flux coefficient
(38)	$w_{ts1,2} = \frac{K_{Lt1,2}B_{g1,2}\tau_{s1,2}}{K_{fe}B_{ts1,2}}$	Stator tooth width
(39)	$d_{s1} = R_{sb1} - R_{PM1} - g_1$	Total slot depth, inner part of the motor
(40)	$d_1 = d_{s1} - \alpha_{sd}w_{ts1}$	Conductor slot depth, inner part of the motor
(41)	$A_s = d_1\left[\theta_s\left(R_{sb1} - \frac{d_1}{2}\right) - w_{ts1}\right]$	Slot area available for conductors
(42)	$R_{sb2} = R_{sb1} + d_{ys}$	Stator back-iron outer radius
(43)	$d_{s2} = R_{os} - R_{sb2}$	Total slot depth, outer part of the motor
(44)	$a = -\alpha_{sd} - \frac{\theta_s}{2}\alpha_{sd}{}^2$ $b = d_{s2} + \alpha_{sd}\theta_s R_{sb2} + \theta_s d_{s2}\alpha_{sd}$ $c = A_s - d_{s2}\theta_s R_{sb2} - \frac{\theta_s}{2}d_{s2}{}^2$	Terms needed for the calculation of w_{ts2}
(45)	$w_{ts2} = \frac{-b\pm\sqrt{b^2-4ac}}{2a}$	Stator tooth width, outer part of the motor

Table 2. *Cont.*

$\mathbf{N_o}$.	Equation	Description
(46)	$d_{ys} = \frac{K_{Lt1}K_{Ltt1}B_{g1}\tau_{p1}+K_{Lt2}K_{Ltt2}B_{g2}\tau_{p2}}{2K_{fe}B_{cs}}$	Stator back-iron width
(47)	$n_s = \mathrm{int}\left(\frac{E_{\max}}{N_m k_d k_p k_s B_{g1,2} L R_{PM1,2} N_{spp}\omega_m}\right)$	Number of turns per slot
(48)	$A_{wire} = \frac{k_{cu}A_s}{n_s}$	Bare area of one winding conductor
(49)	$E_{\max} = \frac{T\omega_m}{i} = N_m k_d k_p k_s B_{g1,2} L R_{PM1,2} N_{spp} n_s \omega_m$	Peak back-EMF
(50)	$I_s = \frac{T}{N_m k_d k_p k_s B_{g1,2} L R_{PM1,2} N_{spp}}$	Peak slot current
(51)	$I_{ph} = \frac{I_s}{N_{ph} n_s}\sqrt{2}$	Phase current
(52)	$J_c = \frac{I_s}{k_{cu}A_s}$	Peak conductor current density
(53)	$R_s = \frac{\rho n_s^2 L}{k_{cu}A_s}$	Slot resistance
(54)	$R_e = \frac{\rho n_s^2 \pi d_{ys}}{2k_{cu}A_s}$	End turn resistance
(55)	$R_{ph} = N_{sp}(R_s + R_e)$	Phase resistance
(56)	$V_{st} = \left[\pi\left(R_{os}^2 - R_{is}^2\right) - 2N_s A_s\right] L k_{fe}$	Stator steel volume
(57)	$P_r = N_{ph} I_{ph}^2 R_{ph}$	Ohmic power loss
(58)	$P_{cl} = \rho_{bi} V_{st} \Gamma(B_{\max}, f_e)$	Core loss
(59)	$\eta_p = \frac{T\omega_m}{T\omega_m + P_r + P_{cl}} 100\%$	Efficiency without mechanical losses

2.1. Design Equations and Methodology

In order to clarify the terminology used in the equations and to allow the reader to become used to the names of the parts of the motor, Figures 1 and 2 present the geometry of both a single and dual-rotor motors.

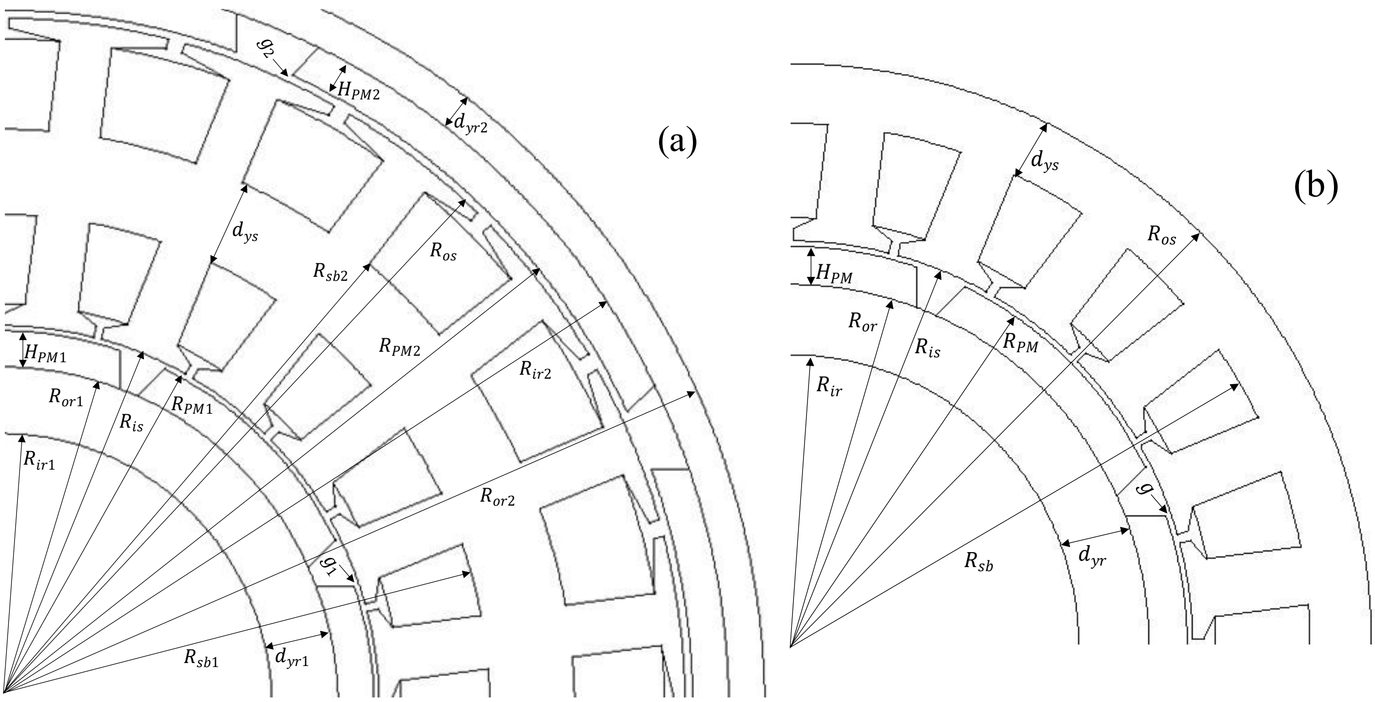

Figure 1. Geometry of radial flux surface-mounted permanent magnet motors. (**a**) Dual-rotor topology. (**b**) Single-rotor topology.

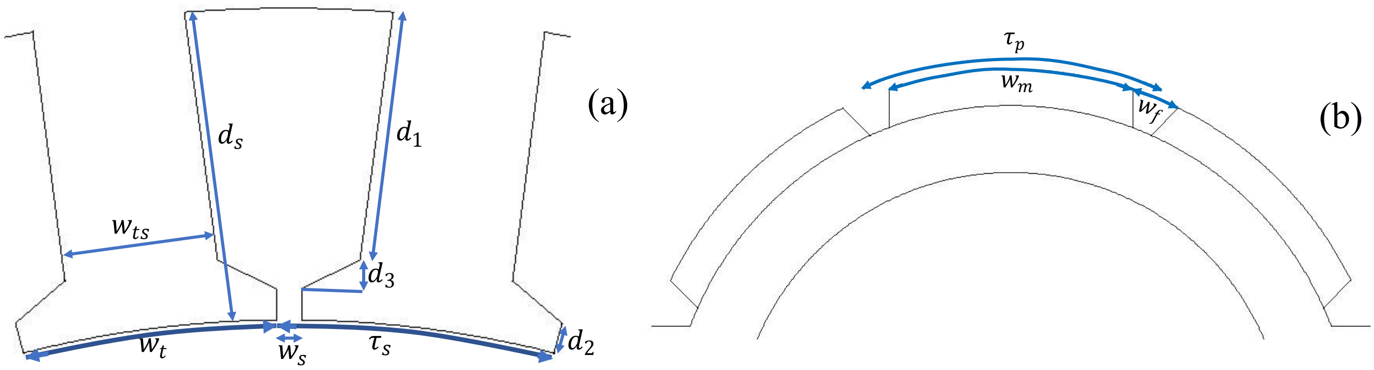

Figure 2. Geometry of stator teeth and rotor magnets. (**a**) Stator teeth. (**b**) Rotor magnets.

Additionally, the winding for the dual-rotor motor was chosen to be toroidal winding, while for the single-rotor motor, conventional single-layer-distributed winding was selected. The reason for using toroidal winding in the dual-rotor topology was that it needed less copper for the conductors compared with traditionally distributed winding, and would also ensure that the current in both the inner and outer parts of the motor would be equal, simplifying the design process. Figures 3 and 4 show both cases and the letters inside the slots indicate the phases.

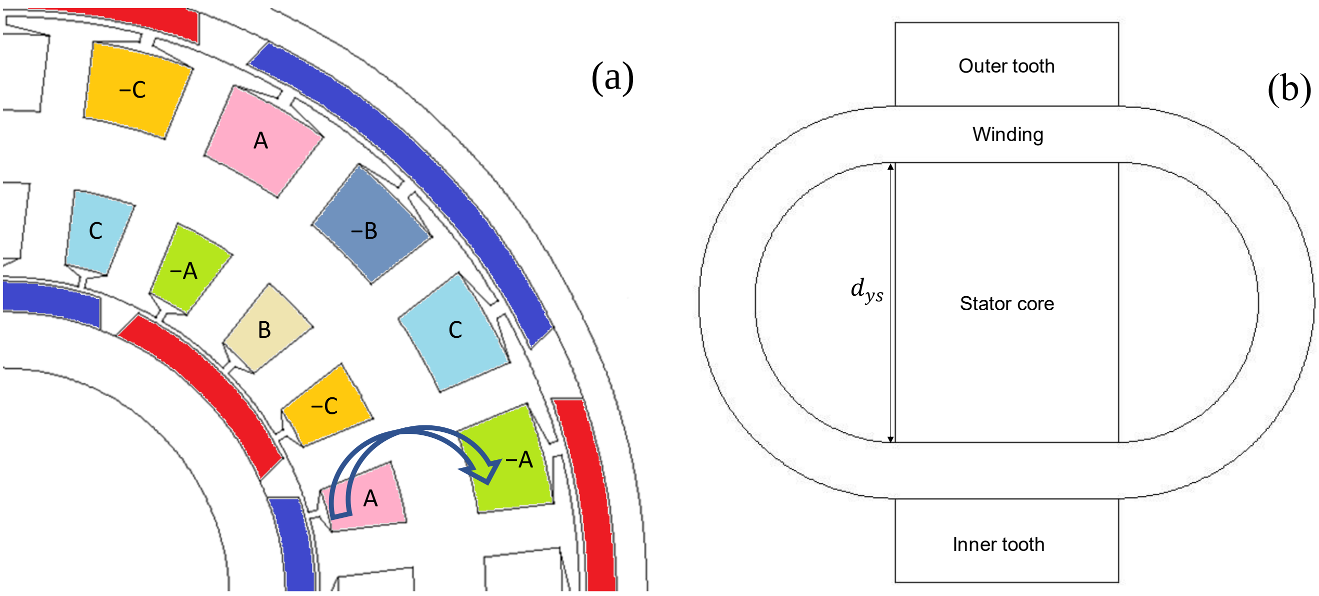

Figure 3. Winding approach for dual-rotor topology. (**a**) Front view. (**b**) Side view.

Now, Table 1 gives the initial parameters needed to start the design process, and Table 2 presents the equations, which were ordered in a way such that they can be evaluated consecutively and result in a complete (but not necessarily optimal) design. The main assumptions considered for the formulation listed in Table 2 were that there was no saturation in the stator nor in the rotors, the magnetic flux from the magnet to the stator and to the rotor were equal, the motor was triphasic and the phase current was sinusoidal. To select the initial parameters, it is recommended to analyze the application for the motor, the materials and resources available, the maximum flux densities of the materials and, if possible, to use the characteristics of other motors employed in similar applications as a guide. It is also important to mention that the equations in Table 2 are for the dual-rotor topology (subscripts 1 and 2 refer to the inner and outer parts of the motor, respectively), but the few changes needed for the single-rotor topology were addressed further in the paper.

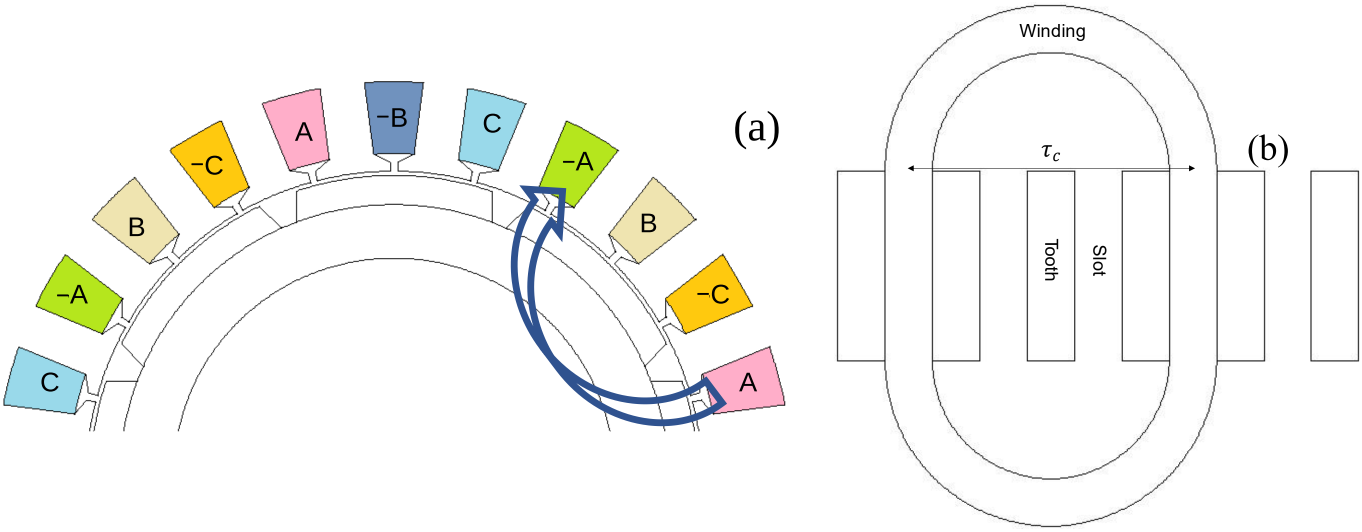

Figure 4. Winding approach for single-rotor topology. (**a**) Front view. (**b**) Top view.

There were some considerations that needed to be mentioned about these design equations. When designing a dual-rotor motor, the inner part should be designed first with the equations from the table and then repeat the process for the outer part, except for the magnitudes meant to be equal in both parts of the motor, like the number of turns per slot, phase current, slot area available for the conductors and phase resistance. Moreover, the output power and the back-EMF should be divided into two parts, since both inner and outer parts of the motor contribute to their value. In the example presented further in the paper, those magnitudes were considered half of the total for the design of each part of the motor, but any other distribution is possible. Additionally, in Equation (47) from Table 2 for the outer part of the motor, the unknown variable was the air gap flux density, so it should be calculated instead of the number of turns.

One important consideration is that Equation (45) from Table 2, which is basically a quadratic formula, may give two different results, but only one can possibly be utilized, because the other would be negative or too large or small for practical use. If no result can be utilized (for example, if both results are negative), R_{PM2} should be modified to be longer so that there is more room in the slots for the tooth width. It is also important to verify the flux density of the outer stator tooth, since its width is not calculated using its desired flux density, but using the area available in the outer part of the motor (Equation (45) from Table 2), and to apply changes to the design parameters if needed to achieve the desired value.

The distribution, pitch and skew factors are only necessary when the number of slots per pole per phase is not 1. Additionally, the angular width of the magnets or the magnet fraction should be chosen in a way such that $\frac{\tau_s}{2} > w_f$, because it is a necessary condition for Equation (37) from Table 2 to be valid. In Equation (30) from Table 2, the variable to calculate is H_{PM}, but a numerical method is needed to solve it. In the same equation, variables η and λ are just meant to simplify the complete expression, so it does not occupy too much space, but when solving for H_{PM}, they and g_e must be substituted using their equations, since they contain the variable H_{PM}. In the case of the shoe depth fraction, values between 0.25 and 0.5 are recommended in [21].

Since Equation (46) from Table 2 needs parameters from the inner and outer parts of the motor, when designing the inner part, an estimation of the values from the outer part is necessary. Considering the values to be equal from both parts is recommended, but it is not mandatory. Later, when such values are available, the stator core flux density should be verified and modifications should be applied if necessary. In this same equation, the flux leakage factor from tooth to tooth K_{Ltt} is considered and can be determined with a finite element analysis, but it is usually small, so it was not taken into account in this paper.

Equation (51) from Table 2 was obtained considering the current as being sinusoidal; therefore, if the current were to have a different waveshape, this equation should be changed, with further information on how to perform this available in [21].

The phase resistance can be calculated only once, because it is the same for the inner and outer parts of the motor, but both are already considered in Equation (57) from Table 2.

For the design of single-rotor motors, the process is easier, since all the extra calculations, parameters and considerations for the outer part of the motor are not present. The design process is similar to that of the inner part of a dual-rotor motor, but some equations need minor changes. Equation (46) from Table 2 would now be $d_{ys} = \frac{K_{Lt} B_g \tau_p}{2K_{fe} B_{cs}}$ and R_{os} could now be calculated using that magnitude with $R_{os} = R_{sb} + d_{ys}$. Due to the toroidal winding, in the dual-rotor motor design, the end turn resistance was calculated using d_{ys}, but in the single-rotor motor, conventional distributed winding was used, so the end turn resistance was calculated with τ_c and the equation changed to $R_e = \frac{\rho n_s^2 \pi \tau_c}{2k_{cu} A_s}$. In Equation (56) from Table 2, multiplying the slot area by two was not necessary anymore, so the new equation became $V_{st} = \left[\pi\left(R_{os}^2 - R_{is}^2\right) - N_s A_s\right] L k_{fe}$. Similarly, the ohmic power loss equation was not necessary to multiply the phase resistance by two, leading to $P_r = N_{ph} \frac{I_{ph}^2}{2} R_{ph}$ because the rms value of the current was originally used here.

2.2. Design of Dual-Rotor and Single-Rotor Motors

Applying the developed methodology, one dual-rotor motor with both rotors in corotation, intended to be used in small electric vehicles like hoverboards, electric bicycles or scooters, was designed. The initial parameters were selected to be similar to those designed in [24–26], and are shown in Table 3.

Table 3. Initial parameters for dual-rotor motor design.

Parameter	Value
P	500 W
η_p	≥90%
S_r	1800 rpm
$E_{\max}$	24 V
N_{ph}	3
N_m	8
N_{sp}	8
g_1	0.6 mm
g_2	2.2 mm
R_{PM1}	70 mm
R_{PM2}	103 mm
R_{sb1}	82 mm
L	20 mm
k_{fe}	0.9
$\Gamma(B_{\max}, f_e)$	1.7 W/kg
ρ_{bi}	7650 kg/m^3
ρ	17.2 nΩ/m
k_{cu}	0.5
α_{mp1}	0.84
α_{mp2}	0.85

Table 3. *Cont.*

Parameter	Value
B_r	0.4 T
B_{cr1}	0.5 T
B_{cr2}	0.514 T
B_{g1}	0.272 T
B_{cs}	1.6 T
B_{ts1}	1.5 T
B_{ts2}	1.5 T
μ_R	1.05
w_{s1}	1 mm
w_{s2}	2 mm
α_{sd}	0.38

A single-rotor motor was designed as well, this time aiming to use the machine as a mini compressor for refrigeration. The main initial parameters were selected considering the information given in [27], and the rest were chosen through trying to achieve a high efficiency. Table 4 shows such parameters.

Table 4. Initial parameters for single-rotor motor design.

Parameter	Value
P	20 W
η_p	≥90%
S_r	1800 rpm
$E_{\max}$	30 V
N_{ph}	3
N_m	4
N_{sp}	4
g	0.35 mm
R_{PM}	22 mm
R_{sb}	37 mm
L	21 mm
k_{fe}	0.9
$\Gamma(B_{\max}, f_e)$	1.7 W/kg
ρ_{bi}	7650 kg/m^3
ρ	17.2 nΩ/m
k_{cu}	0.5
α_{mp}	0.84
B_r	0.4 T
B_{cr}	0.5 T
B_g	0.25 T
B_{cs}	0.8 T
B_{ts}	0.8 T
μ_R	1.05
w_s	1 mm
α_{sd}	0.38

Although the design examples were for low-power motors, the methodology is valid for motors of any power. The results obtained by applying the design methodology were presented in the next section. The simulation of the machines was conducted through an FEA analysis in FEMM (Finite Element method Magnetics) software, version 4.2. The materials used in such simulations were 304 stainless steel for the shaft, M-15 steel for the rotors and stator, regular air for the air gaps, copper for the windings and ferrite for the magnets. About the magnets, one custom type was used, in which the recoil B–H graph was a straight line with a residual flux density of 0.4 T and a coercivity of 380.952 kA/m, which would give a recoil permeability of 1.05.

3. Results

3.1. Dual-Rotor Motor Results

The characteristics and performance obtained from the equations and design process for the dual-rotor motor are presented in Table 5. It could be noted that the results matched the initial parameters, like torque and efficiency.

Table 5. Results from equations for dual-rotor motor.

Variable	Result
f_e	120 Hz
T	2.652 Nm
N_s	24
R_{is}	70.6 mm
R_{os}	100.8 mm
w_{m1}	46.181 mm
w_{m2}	68.762 mm
H_{PM1}	2.7 mm
H_{PM2}	2.7 mm
B_{g2}	0.184 T
d_{yr1}	15.925 mm
d_{yr2}	15.956 mm
R_{or1}	66.176 mm
R_{or2}	122.056 mm
R_{ir1}	50.251 mm
R_{ir2}	106.1 mm
w_{ts1}	3.519 mm
w_{ts2}	3.243 mm
d_{ys}	9.898 mm
A_s	167.353×10^{-6} m^2
n_s	21
I_{ph}	9.773 A
R_{ph}	0.051 Ω
P_r	7.387 W
P_{cl}	7.73 W
η_p	97.065%

Figure 5 was obtained from a simulation, and confirmed that the flux densities were very close to the expected values in all parts of the motor. There were also a few flux lines passing through the slots. The space surrounding the motor was air, but no flux lines passed into it, since the flux density in the outer rotor core was low.

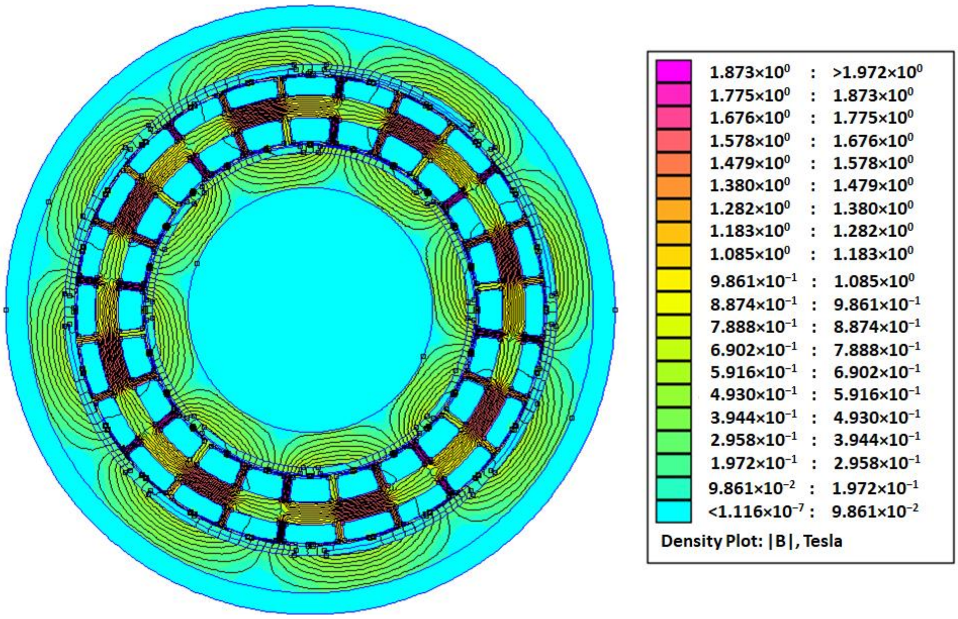

Figure 5. Dual-rotor motor simulation.

Figure 6 shows the load torque and cogging torque of the motor, considering the sum of the contribution of both rotors. Although the average torque of 2.4964 Nm was very close to the calculated value, there was some fluctuation, known as a torque ripple. The acceptable magnitude of a torque ripple depends on each application, but in motors, like the one from [25], less than 10% is good enough. In Figure 6a, the torque ripple was close to 14%, which was a good value considering that the motor had two rotors instead of one. This torque variation was normal in all permanent magnet motors and was caused due to effects like the cogging torque, which is also shown in Figure 6b.

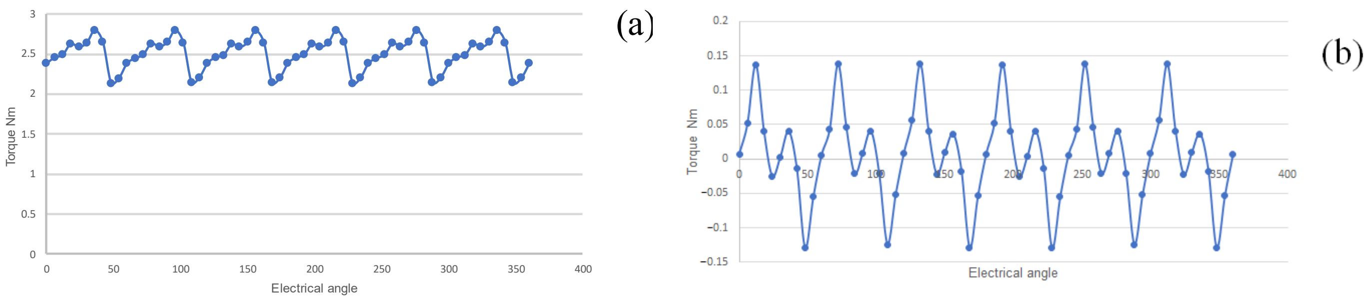

Figure 6. Torque results for the dual-rotor motor. (**a**) Load torque. (**b**) Cogging torque.

The waveform of the back-EMF is shown in Figure 7. The shape was almost sinusoidal and the peak value of 22.87 V was very close to that which was initially calculated. It is important to clarify that the phase currents were simulated as being sinusoidal, so if the current waveforms are different, the generated back-EMF waveform should be different too. This is relevant, because a different phase current may also affect variables like the flux densities, torque ripple and efficiency.

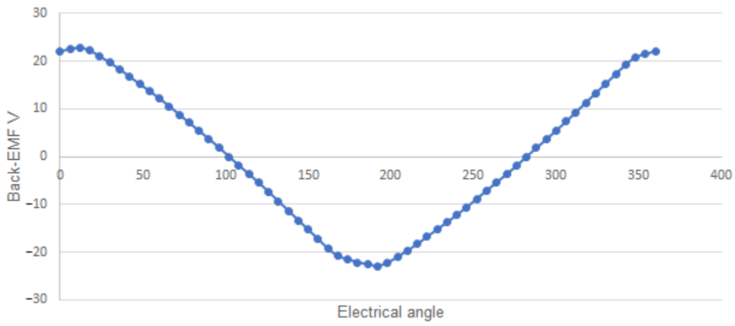

Figure 7. Back-EMF generated with the dual-rotor motor.

Finally, a comparison of the main performance parameters is presented in Table 6. The results showed that the errors were low, which meant that the design methodology was valid for this motor topology. In the case of efficiency, it is important to mention that mechanical loss was not considered, so the real value would be lower. Additionally, the torque ripple was not a parameter established by the designer and the methodology did not address it, but, as mentioned before, 10% is a good value for single-rotor motors, so, in this case, less than 20% was considered acceptable, just like in [28,29], where the torque ripple of the designed dual-rotor motors was approximately 20% before the optimization.

Table 6. Comparison between calculated or expected and obtained results for dual-rotor motor.

Variable	Expected Value	Obtained Value	Error
Torque	2.652 Nm	2.4964 Nm	5.87%
Total air gap flux density (inner and outer part of the motor)	0.456 T	0.437 T	4.12%
Back-EMF	24 V	22.87 V	4.71%
Efficiency	≥90%	97.065%	7.065%
Torque ripple	≤20%	14.37%	5.63%

3.2. Single-Rotor Motor Results

The characteristics and performance obtained from the equations and design process for the single-rotor motor are presented in Table 7. Just like in the case of the dual-rotor motor, it could be noted that the results matched with the initial parameters, like the torque and efficiency.

Figure 8 was obtained from a simulation and confirmed that the flux densities were very close to the expected values in all parts of the motor. In this case, there were no flux lines passing through the slots, probably because of the lower power and characteristics of the machine.

Figure 9 shows the load torque and cogging torque of the motor. The average torque of 109.273 mNm was very close to the calculated value, but there was some fluctuation, as in the case of the dual-rotor design. However, for this motor, the torque ripple was close to 7%, which was an acceptable value considering, again, the information from [25]. The cogging torque is also shown in Figure 9b.

The waveform of the back-EMF is shown in Figure 10. Again, the shape was almost sinusoidal and the peak value of 29.53 V was very close to that previously calculated. The phase currents were simulated as being sinusoidal too.

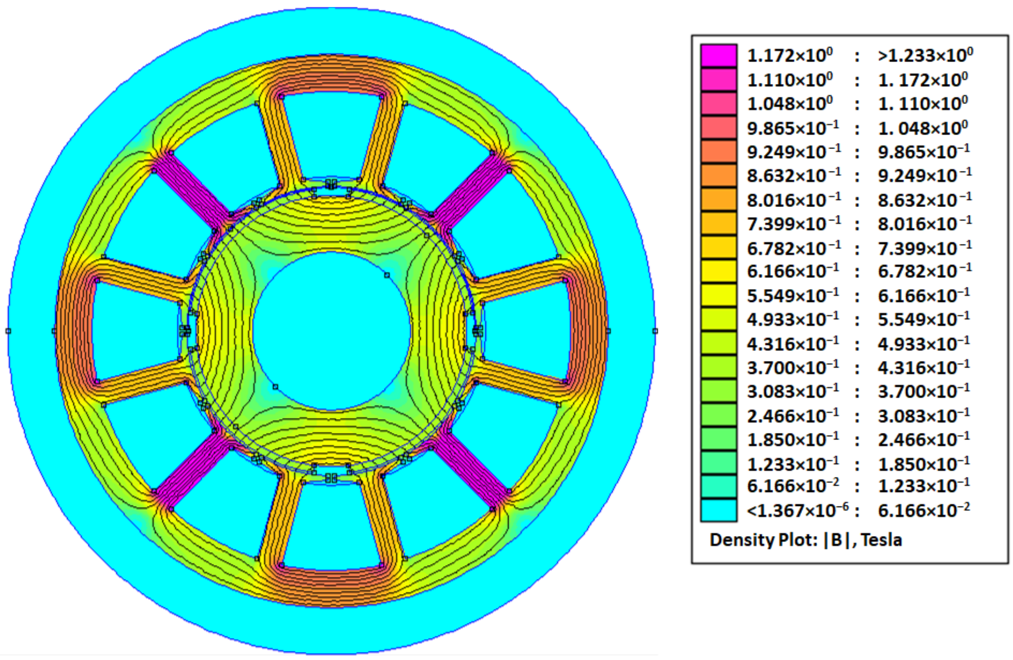

Figure 8. Single-rotor motor simulation.

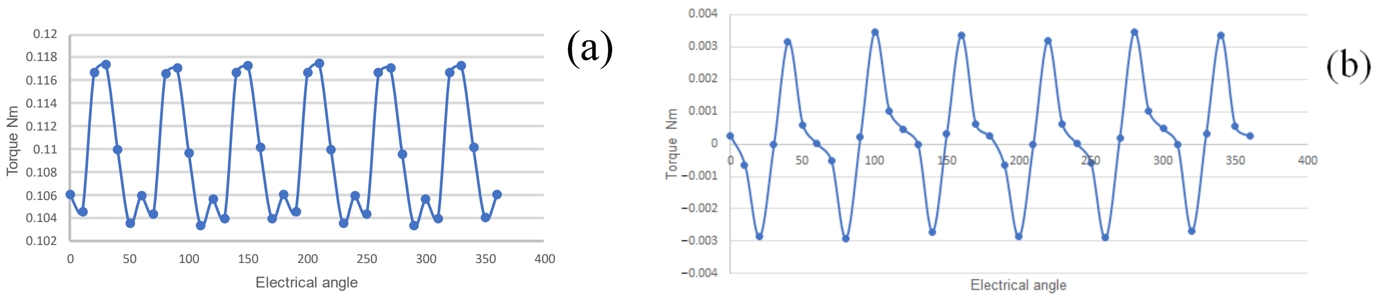

Figure 9. Torque results for the single-rotor motor. (**a**) Load torque. (**b**) Cogging torque.

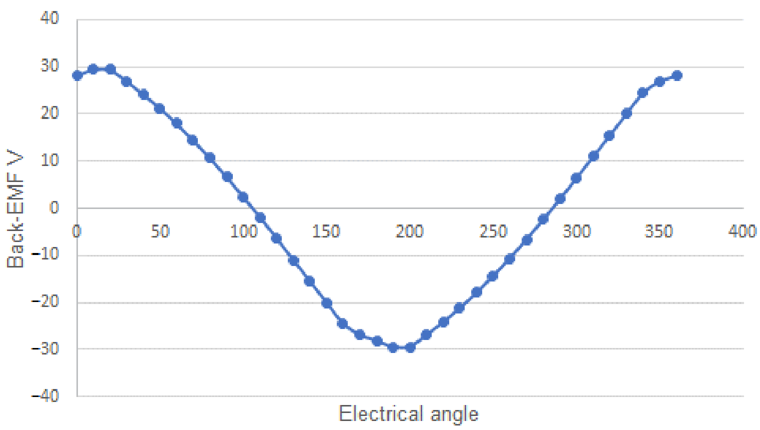

Figure 10. Back-EMF generated with the single-rotor motor.

Table 7. Results from equations for single-rotor motor.

Variable	Result
f_e	60 Hz
T	106.103 mNm
N_s	12
R_{is}	22.35 mm
w_m	29.028 mm
H_{PM}	1.08 mm
d_{yr}	8.71 mm
R_{or}	20.92 mm
R_{ir}	12.21 mm
w_{ts}	3.835 mm
d_{ys}	5.735 mm
A_s	159.418×10^{-6} m^2
n_s	344
I_{ph}	0.315 A
R_{ph}	7.778 Ω
P_r	1.156 W
P_{cl}	0.555 W
η_p	92.119%

Now, Table 8 presents a comparison of the main performance parameters. The results showed that the errors were very low which, meant that the design methodology was valid for this motor topology too. Again, in the case of efficiency, mechanical loss was not considered, so the real value would be lower. Additionally, the torque ripple was not a parameter established by the designer, but, as mentioned before, 10% was considered acceptable.

Table 8. Comparison between calculated or expected and obtained values for single-rotor motor.

Variable	Expected Value	Obtained Value	Error
Torque	106.103 mNm	109.273 mNm	3%
Air gap flux density	0.25 T	0.246 T	1.6%
Back-EMF	30 V	29.53 V	1.57%
Efficiency	≥90%	92.408%	2.408%
Torque ripple	≤10%	7.26%	2.74%

4. Discussion

A design methodology for radial flux surface-mounted permanent magnet motors was developed based on previous studies and validated with a finite element analysis. This methodology was found to be suitable for single-rotor and dual-rotor machines, and is available for researchers to use, in comparison with previous papers, where the design process was not completely shown, so this design's equations and process may be useful, especially for those trying to start in motor design and investigation.

By applying the design equations and process, a 500 W dual-rotor motor and a 20 W single-rotor motor were designed. In both machines, the results of the flux densities, efficiency, average torque and torque ripple were very close to the expected values, as shown in Tables 6 and 8. Especially worth mentioning was the efficiency of both the motors with values above 90%. However, mechanical loss was not considered in this methodology, so the experimental results would be different. Additionally, the efficiency was not directly extracted from the simulator, but calculated from individual results like the flux density, current and wire resistance. The torque ripple was found to be relatively low, with values at approximately 14% and 7%, respectively, and a curious fact to note is that in the dual-rotor motor, the torque ripple was twice that for the single-rotor motor. It would be interesting to investigate more the relation between the torque ripple and the motor topology.

Another result to mention is that the errors between the expected and simulated values were almost twice as high in the dual-rotor motor than in the single-rotor machine. Investigating the causes of this would be interesting as well.

The back-EMF waveforms were almost sinusoidal in these specific cases, mainly because of the sinusoidal currents set in the simulator, since the design and geometry were chosen to allow such a result. However, the causes of the back-EMF not being completely sinusoidal despite the current and design should be investigated.

In this paper, only machines with integer slot/pole numbers were designed, so motors with fractional slot/pole numbers could be designed using the developed methodology in future research. Additionally, since all the currents were simulated as being sinusoidal, another aspect of future research would be the investigation of the effect of different current waveforms and different, or even nontypical, test environments in the performance of motors designed with this methodology. The behavior during the start and the transient response data, like the torque steps and speed ramp, is important for future works as well. The effect of the different winding approaches may be interesting to investigate as well. Moreover, parameters like the stator resistance and d–q axis inductance were not addressed in this paper, so they remain as interesting topics for a future investigation.

It is important to mention that this methodology is a general design process, which means that it is not focused on any specific parameter or goal. This allows researchers to develop their own methodologies depending on their needs or what they want to achieve, like creating designs that keep specific parameters fixed or optimizing the general methodology to, for example, obtain a high efficiency, high torque density, low torque ripple, etc. All these, along with the comparison between the motors designed using this methodology and others reported in the literature, are interesting topics for future research.

Author Contributions: Conceptualization, S.I.S.-S., M.P.-S. and V.H.O.-P.; methodology, S.I.S.-S., S.E.D.L.-A. and C.C.-G.; validation, S.I.S.-S., A.C.-S. and C.C.-G.; formal analysis, S.I.S.-S., M.P.-S and C.C.-G.; investigation, S.I.S.-S., S.E.D.L.-A. and C.C.-G.; writing—original draft preparation, S.I.S.-S. and M.P.-S.; writing—review and editing, M.P.-S., A.C.-S. and C.C.-G.; supervision, M.P.-S., S.E.D.L.-A., A.C.-S. and V.H.O.-P. All authors have read and agreed to the published version of the manuscript.

Funding: This work was supported by the National Council of Science and Technology (CONACYT).

Data Availability Statement: No new data were created or analyzed in this study. Data sharing is not applicable to this article.

Conflicts of Interest: The authors declare no conflict of interest.

References

1. Sanguesa, J.A.; Torres-Sanz, V.; Garrido, P.; Martinez, F.J.; Marquez-Barja, J.M. A Review on Electric Vehicles: Technologies and Challenges. *Smart Cities* **2021**, *4*, 372–404. [CrossRef]
2. de Almeida, A.T.; Fong, J.; Falkner, H.; Bertoldi, P. Policy options to promote energy efficient electric motors and drives in the EU. *Renew. Sustain. Energy Rev.* **2017**, *74*, 1275–1286. [CrossRef]
3. Bouloukza, I.; Mordjaoui, M.; Kurt, E.; Bal, G.; Ökmen, C. Electromagnetic design of a new radial flux permanent magnet motor. *J. Energy Syst.* **2018**, *2*, 13–27. [CrossRef]
4. Jung, Y.-H.; Park, M.-R.; Lim, M.-S. Asymmetric Rotor Design of IPMSM for Vibration Reduction Under Certain Load Condition. *IEEE Trans. Energy Convers.* **2020**, *35*, 928–937. [CrossRef]
5. Karnavas, Y.L.; Chasiotis, I.D.; Korkas, C.D.; Amoutzidis, S.K. Modelling and multiobjective optimization analysis of a permanent magnet synchronous motor design. *Int. J. Numer. Model. Electron. Netw. Devices Fields* **2017**, *30*, e2232. [CrossRef]
6. Kim, J.-H.; Seo, J.-M.; Jung, H.-K.; Won, C.-Y. Analysis and Design of a Novel-Shape Permanent Magnet Synchronous Motor for Minimization of Torque Ripple and Iron Loss. *J. Magn.* **2014**, *19*, 411–417. [CrossRef]

7. Koo, B.; Kim, J.; Nam, K. Halbach Array PM Machine Design for High Speed Dynamo Motor. *IEEE Trans. Magn.* **2021**, *57*, 1–5. [CrossRef]
8. Kwon, J.-W.; Li, M.; Kwon, B.-I. Design of V-Type Consequent-Pole IPM Machine for PM Cost Reduction With Analytical Method. *IEEE Access* **2021**, *9*, 77386–77397. [CrossRef]
9. Park, J.; Paul, S.; Chang, J.; Hwang, T.; Jongsu, Y. Design and comparative survey of high torque coaxial permanent magnet coupling for tidal current generator. *Int. J. Electr. Power Energy Syst.* **2020**, *120*, 105966. [CrossRef]
10. Scuiller, F.; Becker, F.; Zahr, H.; Semail, E. Design of a Bi-Harmonic 7-Phase PM Machine with Tooth-Concentrated Winding. *IEEE Trans. Energy Convers.* **2020**, *35*, 1567–1576. [CrossRef]
11. Shi, Z.; Sun, X.; Cai, Y.; Xiang, T.; Chen, L. Design optimisation of an outer-rotor permanent magnet synchronous hub motor for a low-speed campus patrol EV. *IET Electr. Power Appl.* **2020**, *14*, 2111–2118. [CrossRef]
12. Wu, S.; Zhao, X.; Jiao, Z.; Luk, P.C.; Jiu, C. Multi-Objective Optimal Design of a Toroidally Wound Radial-Flux Halbach Permanent Magnet Array Limited Angle Torque Motor. *IEEE Trans. Ind. Electron.* **2017**, *64*, 2962–2971. [CrossRef]
13. Yang, Y.; Castano, S.M.; Yang, R.; Kasprzak, M.; Bilgin, B.; Sathyan, A.; Dadkhah, H.; Emadi, A. Design and Comparison of Interior Permanent Magnet Motor Topologies for Traction Applications. *IEEE Trans. Transp. Electrif.* **2017**, *3*, 86–97. [CrossRef]
14. Yazdan, T.; Humza, M.; Ali, Q.; Hussain, A.; Kwon, B.-i. Design and analysis of a two-phase brushless DC motor with hybrid permanent magnet material for only-pull drive technique. *Electr. Eng.* **2021**, *103*, 2335–2343. [CrossRef]
15. Kim, S.-m.; Jung, W.-S.; Kim, W.-H.; Bang, T.-K.; Lee, D.-H.; Kim, Y.-J.; Choi, J.-Y. Optimal Design of Permanent Magnet Synchronous Machine Based on Random Walk Method and Semi 3D Magnetic Equivalent Circuit Considering Overhang Effect. *Energies* **2022**, *15*, 7852. [CrossRef]
16. Li, X.; Sun, Z.; Sun, W.; Guo, L.; Wang, H. Design of Permanent Magnet-Assisted Synchronous Reluctance Motor with Low Torque Ripple. *World Electr. Veh. J.* **2023**, *14*, 82. [CrossRef]
17. Qu, C.; Guo, Z.; Hu, Y.; Wang, X.; Han, F. Multi-Objective Optimization Design of a New Permanent Magnet Synchronous Motor Based on the Taguchi Method. *Energies* **2022**, *15*, 7347. [CrossRef]
18. Wang, Z.; Tian, W.; Zhao, W. Magnet Slotting Design to Reduce High Order Electromagnetic Force and Vibration of Permanent Magnet Motor. *Energies* **2022**, *15*, 8684. [CrossRef]
19. Xu, J.; Zhang, L.; Meng, D.; Su, H. Simulation, Verification and Optimization Design of Electromagnetic Vibration and Noise of Permanent Magnet Synchronous Motor for Vehicle. *Energies* **2022**, *15*, 5808. [CrossRef]
20. Gieras, J.F. *Permanent Magnet Motor Technology: Design and Applications*; CRC Press: Boca Raton, FL, USA, 2009.
21. Hanselman, D.C. *Brushless Permanent Magnet Motor Design*; The Writers' Collective: Cranston, RI, USA, 2003.
22. Ronghai, Q.; Lipo, T.A. Analysis and modeling of air-gap and zigzag leakage fluxes in a surface-mounted permanent-magnet Machine. *IEEE Trans. Ind. Appl.* **2004**, *40*, 121–127. [CrossRef]
23. Ronghai, Q.; Lipo, T.A. Design and parameter effect analysis of dual-rotor, radial-flux, toroidally wound, permanent-magnet machines. *IEEE Trans. Ind. Appl.* **2004**, *40*, 771–779. [CrossRef]
24. Bhat, S.B.; Nikam, S.P.; Fernandes, B.G. Design and analysis of ferrite based permanent magnet motor for electric assist bicycle. In Proceedings of the 2014 International Conference on Electrical Machines (ICEM), Berlin, Germany, 2–5 September 2014; pp. 106–111.
25. Lim, D.; Cho, Y.; Ro, J.; Jung, S.; Jung, H. Optimal Design of an Axial Flux Permanent Magnet Synchronous Motor for the Electric Bicycle. *IEEE Trans. Magn.* **2016**, *52*, 1–4. [CrossRef]
26. Song, B.; Chang, K.; Choi, J. Design of an outer-rotor-type permanent magnet motor for electric scooter propulsion systems. In Proceedings of the 2010 International Power Electronics Conference—ECCE ASIA, Sapporo, Japan, 21–24 June 2010; pp. 2742–2763.
27. Rasmussen, C.B.; Ritchie, E. Variable speed brushless DC motor drive for household refrigerator compressor. In Proceedings of the 1997 Eighth International Conference on Electrical Machines and Drives (Conf. Publ. No. 444), Cambridge, UK, 1–3 September 1997; pp. 128–132.
28. Sun, L.; Cheng, M.; Jia, H. Analysis of a Novel Magnetic-Geared Dual-Rotor Motor With Complementary Structure. *IEEE Trans. Ind. Electron.* **2015**, *62*, 6737–6747. [CrossRef]
29. Sun, L.; Cheng, M.; Tong, M. Key Issues in Design and Manufacture of Magnetic-Geared Dual-Rotor Motor for Hybrid Vehicles. *IEEE Trans. Energy Convers.* **2017**, *32*, 1492–1501. [CrossRef]